CH + Destruction by Reaction With H: Computing Quantum Rates to Model Different Molecular Regions in the Interstellar Medium

ARTICLE *in* THE JOURNAL OF PHYSICAL CHEMISTRY A · JUNE 2015

Impact Factor: 2.69 · DOI: 10.1021/acs.jpca.5b02785 · Source: PubMed

3 AUTHORS:

Stefano Bovino
University of Hamburg
52 PUBLICATIONS **320** CITATIONS
SEE PROFILE

Tommaso Grassi
University of Copenhagen
34 PUBLICATIONS **170** CITATIONS
SEE PROFILE

Franco Gianturco
University of Innsbruck
171 PUBLICATIONS **1,565** CITATIONS
SEE PROFILE

THE JOURNAL OF PHYSICAL CHEMISTRY A

Article

pubs.acs.org/JPCA

CH^+ Destruction by Reaction with H: Computing Quantum Rates To Model Different Molecular Regions in the Interstellar Medium

S. Bovino,[†] T. Grassi,[†] and F. A. Gianturco*[,§,∥]

[†]Institut für Astrophysik Georg-August-Universität, Friedrich-Hund Platz 1, 37077 Göttingen, Germany

[‡]Center for Star and Planet Formation, University of Copenhagen, Østervoldgade 5-7, 1350 Copenhagen, Denmark

[§]Institute of Ion Physics, University of Innsbruck, Technikerstrasse 25, 6020 Innsbruck, Austria

[∥]Scuola Normale Superiore, Piazza de' Cavalieri, 56125 Pisa, Italy

ABSTRACT: A detailed analysis of an ionic reaction that plays a crucial role in the carbon chemistry of the interstellar medium (ISM) is carried out by computing ab initio reactive cross sections with a quantum method and by further obtaining the corresponding CH^+ destruction rates over a range of temperatures that shows good overall agreement with existing experiments. The differences found between all existing calculations and the very-low-T experiments are discussed and explored via a simple numerical model that links these cross section reductions to collinear approaches where nonadiabatic crossing is expected to dominate. The new rates are further linked to a complex chemical network that models the evolution of the CH^+ abundance in the photodissociation region (PDR) and molecular cloud (MC) environments of the ISM. The abundances of CH^+ are given by numerical solutions of a large set of coupled, first-order kinetics equations that employs our new chemical package KROME. The analysis that we carry out reveals that the important region for CH^+ destruction is that above 100 K, hence showing that, at least for this reaction, the differences with the existing laboratory low-T experiments are of essentially no importance within the astrochemical environments discussed here because, at those temperatures, other chemical processes involving the title molecule are taking over. A detailed analysis of the chemical network involving CH^+ also shows that a slight decrease in the initial oxygen abundance might lead to higher CH^+ abundances because the main chemical carbon ion destruction channel is reduced in efficiency. This might provide an alternative chemical route to understand the reason why general astrochemical models fail when the observed CH^+ abundances are matched with the outcomes of their calculations.

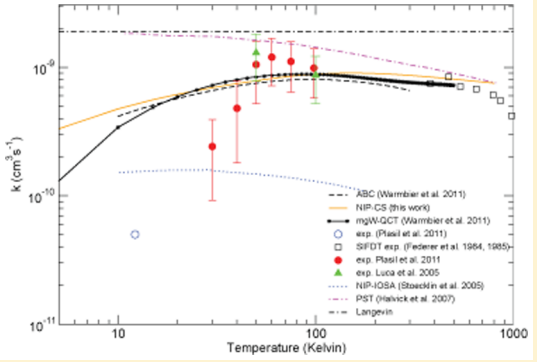

1. INTRODUCTION

The methylidyne cation CH^+ was observed a while ago for the first time[1] in the diffuse ISM and was followed by further detections in a variety of interstellar and circumstellar environments. In its earlier detections, its $A^1\Pi \leftarrow X^1\Sigma^+$ electronic band system was observed,[2,3] whereas the more recent data from the *Infrared Space Observatory*[4] and from the *Herschel Space Telescope*[5] have given access to the far-infrared (FIR) spectrum of this molecule in several remote star-forming regions.[6] The fairly large number of subsequent detections shows that the presence of CH^+ can be considered as confirmed throughout the interstellar matter.[7]

Despite the large effort made by observers to detect with great accuracy the CH^+ bands, this molecule still remains a puzzle in modern molecular astrophysics. The observed averaged abundances, in fact, are still orders of magnitude larger compared to the one provided by astrochemical models, even if some attempts to solve this puzzle came out during the past few years (see discussion below).

The methylidyne has also been known to play a significant role in various steps of the complex chemical network of those molecular processes and reactions that are taken to occur in interstellar and circumstellar regions. For example, its hydrogenation reaction is involved in two important species of that network: the methylene ion CH_2^+ and the methyl cation CH_3^+. Although the latter molecules are found to be rapidly destroyed by efficient dissociative recombination with electrons via

$$CH_3^+ + e^- \rightarrow CH + H_2 \quad (1)$$

$$CH_2^+ + e^- \rightarrow C + H + H \quad (2)$$

they can also react with oxygen and nitrogen atoms forming in addition CO^+, CN^+, HCO^+, and HCN^+ plus other cation precursors of CO, HCN, etc.,[7] thus expected to induce a departure of carbon from its ionization equilibrium.[8] CH^+

Special Issue: Dynamics of Molecular Collisions XXV: Fifty Years of Chemical Reaction Dynamics

Received: March 23, 2015
Revised: June 10, 2015

DOI: 10.1021/acs.jpca.5b02785
J. Phys. Chem. A XXXX, XXX, XXX−XXX

therefore initiates an extensive chemical chain of processes that evolve into the formation of more complex species. The brief outline of reactions given above describes some of the most important paths reported by current astrochemical databases.[9,10] They will also be relevant in our evolutionary modeling reported by section 4.

Because CH^+ is chemically a very reactive ion, its reaction path to destruction by hydrogen abstraction has been considered, together with dissociative recombination and the above hydrogenation processes, one of the important paths for its losses:[11−13] it is thus both important and interesting to assess as accurately as possible the actual efficiency of the following chemical process

$$CH^+ + H \rightarrow C^+ + H_2 \quad (3)$$

so that one may link the above reaction with the extensive variety of chemical processes that come into play when one further models the chemistry of CH^+ in various ISM environments.[7]

In the past few years there have been a series of papers that have dealt first with its photon-induced formation:

$$C^+(^2P_{3/2,1/2}) + H(^2S_{1/2}) \rightarrow CH^+(^1\Sigma^+) + h\nu \quad (4)$$

thereby producing the relevant radiative association rates,[14] and also with the experimental, low-temperature study of its destruction reaction by eq 3 with slow H atoms.[15]

More recently, the formation reaction of CH^+ has been analyzed with new computational data that start from a vibrationally excited ($\nu = 1$) H_2 partner of C^+ and investigate the high-T regimes using a quantum wave packet method.[16]

The above formation reaction 4 is thought to be the main path of CH^+ formation even if a series of other physical processes have to be invoked to excite the H_2 molecules into higher vibrational levels to overcome the endothermicity of the reaction (4177 K). For instance, neutral shocks,[17] and magnetohydrodynamic (MHD) shocks[18] have been suggested earlier but seem to be both ruled out by observations.[19,20] The presence of Alfvén waves[21] and the occurrence of turbulent dissipation[8] still remain viable mechanisms to create vibrationally excited H_2 in diffuse clouds. However, no firm confirmation of its presence or of its possible formation has been obtained thus far. An attempt to provide a model that is able to reproduce the observed abundances has been proposed by Falgarone et al.[6] by exploring turbulent dissipation regions (TDR) in which dissipation of turbulent energy locally triggers a specific warm chemistry. This was found to well reproduce the results for the inner Galaxy conditions. It is not clear that it could also be applied to dark or to diffuse molecular clouds.

The computational analysis of the present reaction has also been carried out by several authors, who employed a variety of reactive potential energy surfaces (RPES) and tried to provide realistic estimates of the reaction rates for the destruction path of eq 3 using a numerical fit of the various surfaces involved. One of the earliest attempts[22] used the infinite order sudden (IOS) approximation for the reaction dynamics, whereas more recent calculations employ a newly computed RPES[23] and used quasi-classical trajectories (QCT) and close-coupling (CC) quantum methods for the dynamics. Another, very recent addition to the calculations of the interaction forces for the CH_2^+ system has been a fully *ab initio* approach that employed a complete active space self-consistent field reference wave function[24] and used a large C(6s5p4d3f)/H(8s6p3d1f) basis set. These calculations focused on the three lowest-lying electronic states that are involved in both formation and destruction of CH^+. Although no quantum dynamical calculations were presented, the three adiabatic RPES allowed for a detailed analysis of the topological features of the possible processes and largely confirmed the shapes of the diabatic descriptions employed by the previous works discussed above.

We therefore decided that it would be still useful to employ the diabatic approach on a single RPES once more, to investigate the destruction reaction 3, but using an accurate quantum method for angular momentum coupling. We further link our findings to a very recent study of Grozdanov and McCarroll[25] and additionally employ our final rates, after a detailed comparison with the experiments and all earlier existing calculations, with a fairly broad chemical network that allows us to model the CH^+ evolution in specific ISM environments. It is therefore the aim of the present work to directly link newly produced quantum reactive cross sections and rates (after their quality assessment in comparison with existing experiments) to an evolutionary modeling that employs a large number of networked reaction involving the title system and looks into the different initial conditions of various ISM environments. To these ends, we decided to employ the lowest diabatic RPES of Warmbier and Schneider[23] and to use our recently developed NIP approach to quantum reactions,[26] where the dynamics was treated within the coupled-states (CS) approach. The use of the NIP method, originally suggested by Baer et al.,[27] had been proved already to be quite realistic when dealing with the many channels which are usually dynamically coupled in ionic reactions[28] and has been shown capable of providing good quality reactive cross sections summed over all possible final states. We shall specifically show below that the present results turn out to provide the best overall agreement with the existing experiments over a broad range of temperatures.

The additionally novelty of the present study, as briefly mentioned above, is that we decided to employ our computed rates, as well as all previously computed rates for the CH^+ chemical destruction by H atoms, within an extensive evolutionary modeling of CH^+ relative abundances within different interstellar medium scenarios. To this end, in fact, we have selected several initial conditions, have linked within the network several chemical reactions taken from current astrochemical databases (see below), and have solved with the publicly available package KROME (www.kromepackage.org) an extensive set of coupled kinetics equations.

The following section briefly describes the main features of the employed RPES, together with an outline of our computational method for yielding reactive cross sections and rates. Section 3 presents our computed quantities and their low-T behavior. It further carries out an interesting comparison with a very recent computational modeling of nonadiabatic effects[25] as well as a detailed comparison with the existing experiments and all the earlier calculations. Section 4 additionally analyses in depth the effects of our computed rates within realistic evolutionary chemical models of molecular regions of the ISM, which include a fairly large network of reactions. The present conclusions are finally given in section 5.

2. QUANTUM DYNAMICS

The CH_2^+ reactive system is characterized by the presence of a conical intersection between the $^2\Sigma^+$ and the $^2\Pi$ PES.[22,23,29] The latter becomes avoided crossing for near-linear, bend

DOI: 10.1021/acs.jpca.5b02785
J. Phys. Chem. A XXXX, XXX, XXX−XXX

configurations and further disappears when the molecule is clearly bent. This behavior has been discussed in great detail in the above studies and will not be repeated here. By performing a diabatization of the relevant RPES, one can obtain a smoother description of the lower, approximately diabatic RPES that we have employed in the present work. This simplification was also done in all the existing previous computational studies, and therefore, we thought it to be in line with all existing comparison with experiments. The resulting angular shape of this diabatized RPES could be seen from the data in Figure 1,

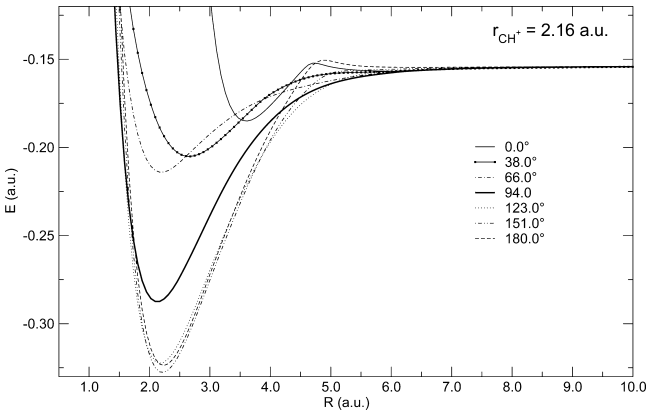

Figure 1. Cuts of the PES at different angles for the CH^+ molecule at its equilibrium distance.

where different cuts are shown for the CH^+ molecule at its equilibrium geometry. We note there that at angles of 0° or 180° (linear configurations) a small barrier occurs around 5 au, obviously depicting the presence of the avoided crossing regions. In our calculations we employ the RPES provided by Warmbier and Schneider,[23] constructed following a modified ansatz.[30−32] This RPES is better in terms of accuracy than that in the previous work[22] for two main reasons: (i) the number of points used to construct it is 16259 to be compared with 3291 used by the earlier authors, and (ii) the global root-mean-square found here is 15.5 meV to be compared with the 59.4 meV value of Stoecklin and Halvick.[22] It should be added that, in both cases similar results for the two fragments (CH^+ and H_2) diatomic curves are provided, also in good agreement with experiments. Furthermore, the RPES of Warmbier and Schneider[23] provides a fitting that is more accurate in the complex's region (CH_2^+), the latter being very important in terms of reactive scattering studies involving ionic species because they indeed proceed largely through the complex's formation regions. An additional set of polynomials has been included for each intersection: as stated by the authors, this approach is very sensitive to the chosen parametrization but offers a more accurate description of the conical intersections when compared to the global accuracy of the whole potential fit.[23]

To describe the full dynamics of the reaction in eq 3, given the RPES features outlined above, becomes computationally very demanding because it should be solved by taking into account the presence of at least two different PESs. In practice, all published calculations thus far have resorted to using a single diabatic RPES, arguing that to be a realistic choice given the translationally cold regimes that are relevant for the ISM environments. They all considered the lower portion only of the conical intersection region and of both reagents' and products' states.

A recent publication[25] has analyzed within a modified statistical model the possible effects of the conical intersections at the collinear orientations, and we shall discuss their findings below, showing them to be in line with our own model analysis of such effects, also detailed below.

The earliest computational/theoretical data related to this reaction have been obtained by employing methods that use an asymptotic basis expansion and some approximation in the dynamics. The negative imaginary potential (NIP) calculations reported by Stoecklin and Halvick[22] include the IOS approximation that is generally known to underestimate the reactive cross sections,[33] whereas the subsequent work by Halvick et al.[29] employed a quasi-classical trajectory (QCT) and phase-space theory (PST) methods that are expected to be inaccurate at very low temperatures, where the quantum mechanical effects are dominant, as will be shown below. The later work by Warmbier and Schneider[23] used a more accurate RPES and more accurate dynamics, which involved the close-coupling (CC) ABC code[34] and explored the first five rotational levels for the CH^+ molecule.

Our approach is based on the NIP method introduced by Baer et al.[27] and extended in our previous works[26,28,35] (see these papers for the mathematical details), which made use of an additional potential term, V_{NIP}, aimed at absorbing the reactive flux. Because of the flux-absorbing effects coming from it, the resulting **S**-matrix is nonunitary and its default to unitarity yields the (state-to-all) reaction probability, as discussed in Tacconi et al.[26]

$$P^{J\Omega}_{(a\rightarrow \mathrm{all})} = 1 - \sum_b |S^{J\Omega}_{ab}|^2 \tag{5}$$

From the reaction probability $P^{J\Omega}$ one can in turn obtain the reactive cross section

$$\sigma(E) = \frac{\pi}{(2j+1)k^2} \sum_J \sum_\Omega (2J+1) P^{J\Omega}_{(a\rightarrow \mathrm{all})} \tag{6}$$

evaluated from a given initial state (ν, j) and summed over all the final roto-vibrational states of the products. In eq 6 E is the collision energy, k is the wave vector, J is the total angular momentum, and Ω is the projection of the rotational angular momentum along the body fixed (BF) axis. Once the reactive cross sections are obtained, the rate coefficients are computed by averaging the appropriate cross sections over a Boltzmann distribution of relative velocities:

$$\alpha(T) = \frac{1}{(k_B T)^2} \sqrt{\frac{8k_B T}{\pi\mu}} \int_0^\infty \sigma(E) e^{-E/k_B T} E \, dE \tag{7}$$

where T is the gas temperature, k_B is the Boltzmann constant, and μ is the reduced mass of the system.

It is important to note here that our NIP implementation is different from the one discussed by Stoecklin and Halvick,[22] where an asymptotic basis for the roto-vibrational CH^+ states is used throughout the entire reactive domain. In addition, their calculations employ the IOS approximation[36] that treats the rotational motion as "frozen" during the collisions so that the final cross sections are evaluated at fixed Jacobi angles. In our approach an adiabatic basis set is employed instead for the expansion of the scattering wave function, thus taking into account the physical effects by which interaction between the incoming atom and the molecule can progressively modify the

DOI: 10.1021/acs.jpca.5b02785
J. Phys. Chem. A XXXX, XXX, XXX−XXX

reagents' rotovibrational states. The reactive scattering calculations are carried out in the BF frame making use of the CS coupling approximation,[37,38] which has been found to provide accurate results when compared with experiments: see the earlier works by Bovino et al.[28,35] It should also be mentioned here that the parameters that describe the spatial extension and the absorbing tail of the negative, absorption potential of the NIP approach have been extensively varied and modified until numerical stability and numerical convergence of the final cross sections at all energies has been achieved. This specific aspect of the method has also been extensively discussed in earlier work by Bovino et al.[28,35] and will also be mentioned below.

3. RATE COEFFICIENTS AND LOW TEMPERATURE BEHAVIOR

3.1. Measured and Computed Rates. We carried out calculations for the reaction in eq 3 starting from the initial roto-vibrational level $\nu = 0, j = 0$ and for energies ranging from 10^{-5} to 1.0 eV. Our results are thus providing final rates between 10 and 1000 K, and therefore extend the range of temperatures sampled by most of the earlier calculations. All the parameters employed here ensured a relative error of the calculated reactive cross sections within 1%. A basis set expansion of 800 functions has been used for the CH^+ reagent, leading to an equal number of coupled equations. The molecular basis functions were expanded over a direct product of a Colbert−Miller discrete variable representation (DVR) of 150 points (ranging from 0.35 a_0 to 15.0 a_0) and a set of 48 spherical harmonics. The convergence over the total angular momentum values (J) has also been checked: we used a number of J ranging from 10 to 42 for the highest energy. Following the earlier criteria[27] we have also obtained the following stable NIP parameters that have been employed in the calculations: $r_{min} = 6.75\ a_0$, $r_{max} = 10.25\ a_0$, and the NIP order $n = 2$ (see ref 26 for further details).

The final rates are shown in Figure 2 where they are compared with previous calculations and with the existing experimental data. As can be seen from that figure, our results are both in good agreement with the accurate ABC−CC calculations that used the same RPES[23] and with the experiments for temperatures above 60 K.[15] It is worth noting here that for temperatures below 60 K the experiments by Plasil et al.[15] are still seen to decrease with temperature faster than any of the available calculations. A possible explanation for such a behavior will be further discussed, while also noting here that an independent set of additional new measurements would be a welcomed addition to the available data. Other computed values obtained with the ABC and QCT methods[23] employing the same RPES are, like us, in good agreement with the experiments, whereas the results from Stoecklin and Halvick[22] and Halvick et al.[29] appear to deviate from both sets of data. This behavior may be attributed both to their specific, dynamical approach (involving a different set of approximations) and to the lower numerical accuracy of the RPES involved.

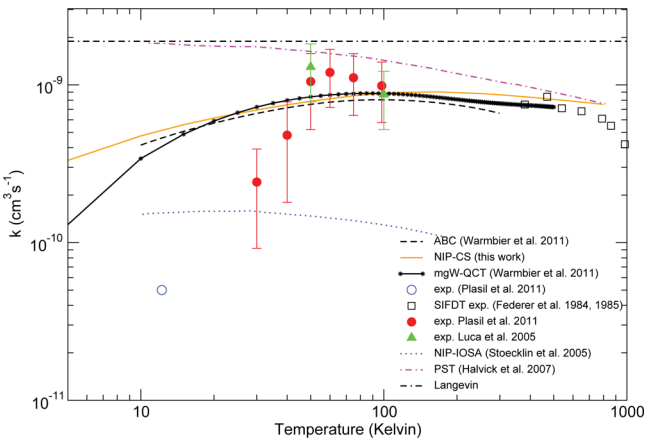

Figure 2. Reaction rates for the destruction channel of eq 3 as a function of the temperature for different calculations and experiments. The data pertaining to the calculations from ref 23 become much denser above 100 K, as shown in the figure. Experimental data from Federer et al.,[39,40] Plasil et al.,[15] and Luca et al.[41] The blue point is part of the results by Plasil et al.[15] but has been evaluated by the authors at slightly different translational and rotational temperatures; see the original paper for details.

We provide here two functional forms for our computed rate coefficient: one considered to be less accurate that follows the classical Kooij form

$$k(T) = \alpha\left(\frac{T}{300}\right)^{\beta} \exp(-\gamma/T) \tag{8}$$

with $\alpha = 8.72 \times 10^{-10}$, $\beta = -0.075$, and $\gamma = 10.1866$, and another, more accurate fit (employed in these calculations) given by

$$k(T) = a\sqrt{T} + bT + cT^{3/2} + dT^2 \tag{9}$$

where $a = 1.9336 \times 10^{-10}$, $b = -1.4423 \times 10^{-11}$, $c = 4.3965 \times 10^{-13}$, and $d = -4.8821 \times 10^{-15}$. Both fits are valid in the range of temperatures from 10 to 1000 K. (The corresponding details of the covariance matrix for the above fitting of the rates can be obtained on request from the authors.)

3.2. Low Temperature Behavior. As already mentioned above, one of the critical results reported by Plasil et al.[15] is the fast drop in the rates at temperatures below 60 K seen by their experiments. Given that the dynamics of the system has been analyzed with different computational methods, we thought that it would be interesting to further explore via a computational "experiment" another possible physical cause for such a feature, because the numerical diabatization artificially introduces a barrier as seen in our Figure 1. More specifically, the presence of the barrier is due to a numerically smoothed out conical intersection occurring for the collinear alignments of the reactants: H−H−C and H−C−H. A very interesting theoretical paper recently published on this subject[25] analyzes the reactive behavior of such collinear configurations within a modified statistical treatment and finds that, by artificially suppressing the reactivity of the rotational states of CH^+ that dominate the reaction at those alignment channels, the final rates drop with temperature more rapidly, although not quite as the experiments. Their conclusions indicate that, if the presence of a barrier after diabatization were to be used to represent reactive flux losses into the other coupled surfaces, then a possible explanation of the existing experiments could be linked to the physical presence of such intersections that dynamically would subtract flux from the diabatic RPES employed by all calculations thus far. To explore this option, we have therefore carried out further model calculations in which we arbitrarily modify that barrier by using a disposable artificial parameter (α) that can increase the barrier

DOI: 10.1021/acs.jpca.5b02785
J. Phys. Chem. A XXXX, XXX, XXX−XXX

height along the crucially important linear configurations. This artificial increase would therefore reduce tunneling of the reagents into the inner region of the reactive lower diabatic surface employed by the calculations, thereby mimicking the losses of dynamical flux from the diabatic channel into the upper surfaces excluded by diabatization.This is indeed the specific aim of our present numerical "experiment" with the arbitrary parameter mentioned above. We have therefore carried out different calculations with different values of that parameter to see how much such artificial changes in the barrier height at the collinear crossings can affect the final cross sections at low energies. In Figure 3 we report the results of our

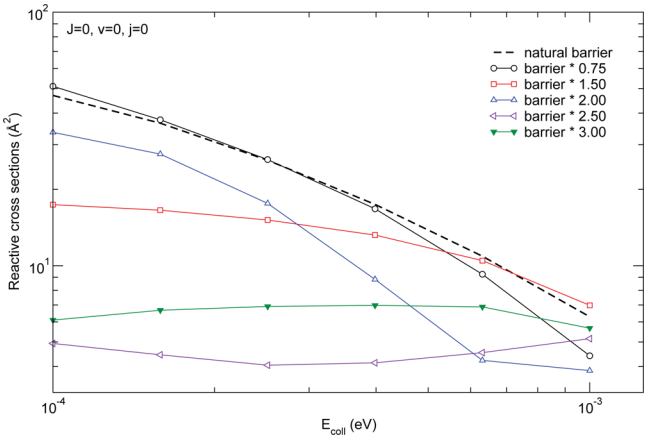

Figure 3. Reactive cross sections as the function of the collision energy for different values of the α parameter. See text for the details.

model for different values of α ranging from 0.7 to 3.0. We can thus see in this figure that an increase of the barrier leads to lower values of the cross sections at low temperatures, whereas for energies larger than 1 meV the differences are not so marked. It should be noted that in this numerical study, because of its modelistic nature, we are testing only the contribution from the most important partial wave ($J = 0$) and that when going to larger energies, the higher J contributions should be added. However, because the behavior at very low energies is largely controlled by the s-wave, this test is a reasonable one to see whether or not there is a clear presence of a correlation between barrier height and reactive probabilities. This fairly simple numerical experiment is therefore telling us that nonadiabtic effects are particularly important at the lower temperatures because the low-T alignment of the reactants would lead to additional flux losses into the other RPES's. As it happens, the low temperature regime is exactly the region were the experiments are showing a marked drop in the size of the cross sections and rates: it therefore follows that our numerical tests in that region have realistically modeled the dynamics by observing the flux losses into different channels induced during the collinear encounters of reactants whenever the tunneling probability into the inner region of the lower diabatic, single RPES is reduced. The results of Figure 3 further suggest that such effects are shown by our present study to become less important as the temperature increases, a feature that we will further discuss below in more detail in relation with the evolutionary calculations. These findings shall thus be very relevant for the analysis, presented in the next section, where we discuss the CH^+ evolution within a large network of linked chemical processes to establish their bearing on the evolutionary abundances of the CH^+ molecule. We shall, in fact, show below that other chemical processes take over at the lower temperatures, thereby making less relevant for the overall chemical evolution the role of the nonadiabatic effects that calculations disregard in the present reaction. Such effects become indeed less important at the higher temperatures, and therefore, we see there that the agreement between our calculations and the experiments, as shown in Figure 3, is indeed quite good: it confirms the general reliability of the single, diabatic RPES approach employed in the present work.

4. CH^+ CHEMISTRY IN DIFFERENT ISM ENVIRONMENTS

We have additionally analyzed the effects of the present rates on an ISM model which selects a specific chemistry based on H, He, C, and O elements, because the above components are the most abundant under the physical conditions that we shall discuss below. We have also introduced metals (Si, S, Fe, Mg, Na, Cl, and their ions) with photoionization and recombination rates using the value provided by the KIDA database. This enhancement does not modify the results described here, confirming the assumption made by the PDR model benchmark where metals are absent: see ref 42.

Due to the ubiquitous presence of the CH^+ molecules we decided to model the evolution of the gas by exploring different environments: from a PDR to a self-shielded molecular cloud (MC). To do that, we essentially vary the extinction coefficient A_v within our model and make it range from 0.2 to 6; we further select the temperature according to what is suggested in section 9.6 of Tielens,[43] thereby selecting an impinging radiation field, G_0, to be equal to 10^5. As indicated above, we employ a subnetwork of the chemistry given in the UMIST database (http://www.udfa.net), which includes 420 reactions and 49 species, the latter chemical species being listed in Table 1. Reactions involving species up to CH_4 (and ions, including

Table 1. List of the Species Included in Our ISM Model (Details in Text)

e^-	H	H^-	H^+
He	He^+	C	C^-
C^+	O	O^-	O^+
H_2	H_2^+	C_2	CO
CO^+	O_2	O_2^+	OH
OH^+	CH	CH^+	HCO
HCO^+	CH_2	CH_2^+	CH_3
CH_3^+	H_2O	H_2O^+	HOC^+
H_3^+	H_3O^+	CH_4	CH_4^+
CH_5^+	Si	S	Fe
Mg	Na	Cl	Cl^+
Si^+	S^+	Fe^+	Mg^+
Na^+			

CH_5^+ and H_3O^+) are taken from the KIDA database (http://kida.obs.u-bordeaux1.fr/). From the species listed in our Table 1 one can therefore reconstruct the full reaction network we have employed and obtained from the KIDA and UMIST databases.

It is worth noting that some of the rate coefficients in the UMIST database have a limited temperature range of applicability which is mainly focused to the cold regions ($\lesssim$300 K). We therefore extended such rate coefficients to cover a wider temperature range, following (whenever possible)

DOI: 10.1021/acs.jpca.5b02785
J. Phys. Chem. A XXXX, XXX, XXX−XXX

the indications from the works where the rates had been evaluated.

4.1. Employed Kinetics Equations. To follow the time evolution of a set of initial species that interact via a given set of reactions, we need to solve a system of ordinary differential equations (ODEs). The ODE associated with the variation of the number density of the ith species is

$$\frac{dn_i}{dt} = \sum_{j \in F_i} \left(k_j \prod_{r \in R_j} n_r(j)\right) - \sum_{j \in D_i} \left(k_j \prod_{r \in R_j} n_r(j)\right) \quad (10)$$

where the first sum represents the contribution to the differential by the reactions that form the ith species and the second part is the analogous for the reactions that destroy the ith species. Each reactant R_j at a given time t has an abundance in number density which is $n_r(j)$, and the corresponding reaction rate coefficient is k_j, which is a function of the gas temperature, but it can be a function of any parameter, including the number densities. Depending on the number of species in the given reactions network a set of coupled first-order ODEs should be solved. In this work we employ the publicly available package KROME.[44]

4.2. Initial Conditions. We performed a series of standard one-zone models with different temperatures and different visual extinction coefficient values (A_v) according to Figure 4.

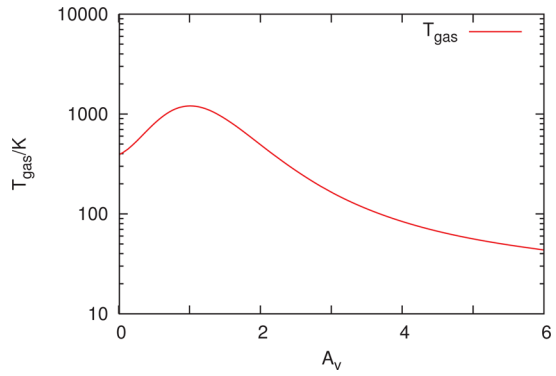

Figure 4. Temperature profile as a function of the extinction coefficient. Adapted and created from a present fitting of the data from ref 43 section 9.6, Figure 9.7.

In each model we take the temperature and density to be constant quantities during the evolution at a given A_v, and the chemical species are computed within a nonequilibrium scheme by using the chemical package KROME[44] that employs a DLSODES solver.[45] The initial conditions for the selected chemical species are given in Table 2 as fractional abundances with respect to the total hydrogen number density $n_{Htot} = 2.3 \times 10^5$ cm^3, whereas for the free electrons we adopt $n_e = \sum_i n_i$ where n_i are the ions abundances,[46−48] to ensure overall charge neutrality. Finally, the cosmic rays ionization rate is set to 1.3×10^{-17} s^{-1}

Table 2. Initial Fractions with Respect to n_{Htot}

species	fraction	species	fraction
H_2	0.50	He	9.00×10^{-2}
O	2.56×10^{-4}	C^+	1.20×10^{-4}
S^+	1.5×10^{-5}	Si^+	1.7×10^{-6}
Fe^+	2×10^{-7}	Na^+	2×10^{-7}
Mg^+	2.4×10^{-6}	Cl^+	1.8×10^{-7}
e^-	see text		

in all the models, and we do not include any cooling or heating term during the 10^8 years evolution that we have sampled, to specifically assess the expected role of the chemical reactions included in our network. This last assumption implies, for a given A_v, a constant temperature during the chemical evolution (e.g., see ref 48).

4.3. Results. The results of our calculations are shown in Figure 5, where we present the CH^+ fractional abundances,

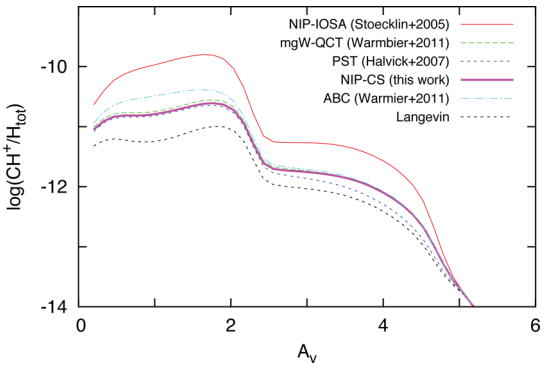

Figure 5. Fractional abundances of the CH^+ molecule normalized to the total density of the gas as a function of the visual extinction A_v. We present different profiles for different choices of the computed destruction rates discussed in the present work (see text for details).

given by all the calculated rates presented in Figure 2, as a function of the visual extinction A_v, the latter going from 0.2 to 6. This range of values influences the photoionization and photodissociation rate coefficients that in the UMIST database have the form $k = \alpha \exp(-\gamma A_v)$ in units of s^{-1}, where α and γ are two parameters that depend on the reaction considered. As indicated in the database documentation, the rate coefficients are computed by integrating the radiation field of Draine[49] multiplied by the cross section of the process being considered, and an exponential factor that takes into account the opacity, a quantity that in turn is a function of A_v (e.g., see ref 50).

The amount of CH^+ shown in Figure 5 is markedly higher in the region with lower A_v, where the dominant formation path is controlled by the endothermic (4177 K) reaction[16]

$$H_2 + C^+ \rightarrow CH^+ + H \quad (11)$$

that is considered to be more efficient at the higher temperatures (lower A_v). On the contrary, within the MC-like regions (higher A_v) where the temperature becomes lower the rate coefficient for eq 11 is no longer efficient. In the region around $A_v \approx 2.2$ the profile presents a slow decrease that is most evident at that value of A_v, and the fractional abundance further slowly decreases and becomes negligible when it reaches values beyond ∼5.2 of the visual extinction. From an analysis of our calculations we found that the decrease around $A_v \approx 2.2$ is due to the concurrent increase of the H_2O abundance which depletes the C^+ abundance and hence reduces the efficiency of the molecular ion's formation by eq 11. In the specific network employed here, this competing process is, in fact, triggered by the following endothermic reaction with oxygen

$$H_2 + O \rightarrow OH + H \quad (12)$$

that produces the OH molecule, which in turn feeds the reaction

$$H_2 + OH \rightarrow H_2O + H \quad (13)$$

DOI: 10.1021/acs.jpca.5b02785
J. Phys. Chem. A XXXX, XXX, XXX−XXX

and finally the H_2O produced is additionally further involved in the reactions

$$H_2O + C^+ \rightarrow HCO^+ + H$$
$$\rightarrow HOC^+ + H \quad (14)$$

that consume the C^+ ion, the latter being the main source of CH^+ within the present modeling and is indicated by eq 11. To numerically test the above chain of reactions we found, in fact, that when we reduce the initial abundance of the atomic oxygen by a factor of 2 in our network, the more marked decrease of the fractional abundances around A_v 2.2 is reduced and the amount of CH^+ markedly increases, especially in the optically thick region ($A_v \gtrsim 3$) corresponding to lower temperatures. This numerical experiment therefore confirms the suggested role of the above reactions within the chemistry of CH^+ and of CH_2^+. It is interesting to note here that a recent publication[51] revealed in the spectral mapping of the helix nebula NGC7293 extended CO photodissociation and OH^+ emission and linked the chemical chains we employ here to the oxygen and neutral carbon presence in that environment. They explicitly refer to the H_2O observation from its fundamental line at 557 GHz, which provides additional, and independent, support to our comments on the possible destruction of C^+ by H_2O via eq 14. The importance of some cation-like HCO^+ in such environments has been also pointed out by Mladenović and Roueff.[52]

The results that we report in Figure 5 are obtained using the fitting given in eq 9. We also present in that figure the comparison between the behaviors of all the different fractional abundances that can be obtained within our modeling when the various rate coefficients discussed in section 3 and shown in Figure 2 are used. We complete the comparison by also reporting the Langevin value $k_{LV} = 1.89 \times 10^{-9}$ cm^3 s^{-1} which we obtained by following ref 53. The more marked differences are found at lower A_v when either the NIP-IOS calculations or the Langevin rate coefficients are used. As expected, the latter rate is an upper limit for all the computed reaction coefficients and therefore produces at the higher temperatures the least amount of CH^+. On the contrary, the rate coefficient from Stoecklin and Halvick,[22] which employs an approach expected to fail more at the lower temperatures, is seen here to depart from our findings over the whole range of temperatures (A_v).

It is also useful to note that the differences at the lower A_v do not originate from the discrepancies of the rates at low temperature discussed in section 3 but rather depend on the high temperature conditions at these extinction coefficient values (Figures 2 and 4) where even the PST and the QCT rate calculations produce reasonable results, although the PST is failing at lower temperatures as expected. To better understand this behavior, we show the evolution of the velocities of the main reactions for the destruction of the CH^+ molecule at two different A_v conditions: one representing a PDR-like environment ($A_v = 0.5$, $T_{gas} \approx 800$ K) and another describing a MC-like ($A_v = 6$, $T_{gas} \approx 50$ K) environment. The velocity ϵ_i of the reaction is defined as

$$\epsilon_i = \frac{k_i n_{r1i} n_{r2i}}{\max(k n_{r1} n_{r2})} \quad (15)$$

where k_i is the rate coefficient, n_{r1i} and n_{r2i} are the abundances of the reactants, and the denominator represents the velocity of the fastest destruction rate at a given time. These quantities are reported in Figures 6 and 7, for $A_v = 0.5$ and $A_v = 6$, respectively. To further emphasize the differences with earlier

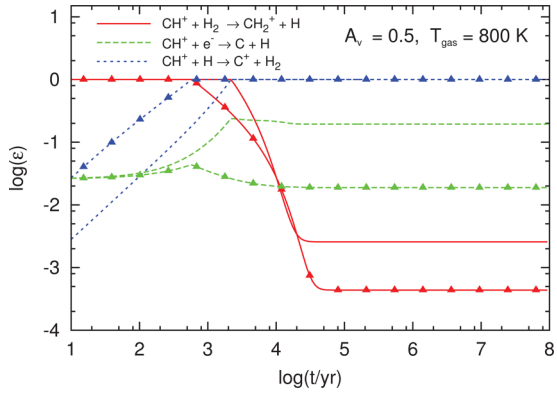

Figure 6. Evolution of the velocities of the main CH^+ destruction reactions normalized to the most important one for $A_v = 0.5$. The two sets of curves refer to the results obtained from the present rate calculations (marked with triangles) and to those obtained from the rates of Stoecklin and Halvick,[22] already discussed in section 3.

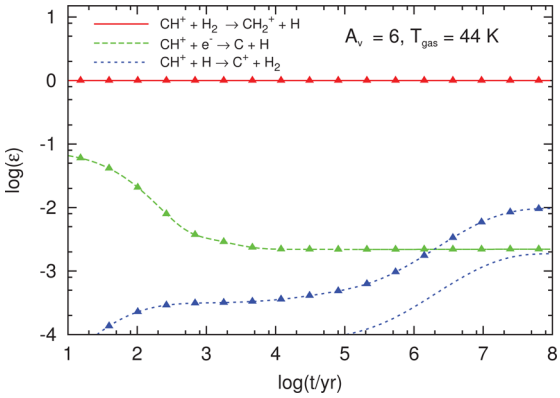

Figure 7. Same as Figure 6, but for $A_v = 6$.

calculations already presented in Figure 5, we show in Figure 6 the evolution of the velocities of the destruction reaction also done via the rates computed by Stoecklin and Halvick.[22] In the optically thin regime, where the photodissociation of H_2 is more efficient, we can see in the figure that the reaction

$$H_2 + CH^+ \rightarrow CH_2^+ + H \quad (16)$$

dominates the CH^+ destruction, whereas, when the hydrogen becomes atomic, the channel of eq 3 starts to be important. The optically thick environment (Figure 7) is dominated by the presence of H_2 during the whole evolution, and therefore the reaction of eq 16 always plays a key role. These plots clearly show that in the lower temperature region, where the computed rates are markedly different from one another (Figure 2), the results are seen to be only marginally influenced by such differences because this destruction channel becomes in fact negligible. Conversely, at the expected higher temperatures of the PDR-like environment, the smaller differences between the rates arise because this new environment is now becoming richer in atomic hydrogen at the later temporal stages (Figure 6). In addition, from Figures 6 and 7 we note that, given our selected initial conditions and the chemical network we have employed, the dissociative recombination is not likely to be important for the destruction of the CH^+ molecule when compared to the other existing destruction channels.

DOI: 10.1021/acs.jpca.5b02785
J. Phys. Chem. A XXXX, XXX, XXX−XXX

5. CONCLUSIONS

In the present work we have attempted to address various, separate aspects involving the chemistry of the CH^+ in the ISM, combining them together to gain a better understanding of its role as a chemical component in many diverse environments:

(i) We have carried out a new theoretical evaluation of the chemical path to its destruction via the chemical reaction with H atom (eq 3).

(ii) We have employed the computed reaction rates within different time-dependent one-zone models of CH^+ exploring either a PDR-like, high-temperature environment or a MC-like model at lower temperatures.

(iii) We have carried out numerical modeling tests on the features of the employed single RPES in the region of the conical intersections to show that reactive flux losses into the other coupled RPES's could be relevant at the very-low temperatures. This could partly explain the experimentally observed drops in rate values as T decreases. More calculations that would explicitly employ several RPESs in the dynamical treatment are clearly needed to better clarify this point.

(iv) The present time-dependent study of a large set of connected chemical reactions clearly shows that the above, low-T regime of reaction 3 is marginally affecting the CH^+ presence in the astrophysical environments that we have modeled, because under those conditions other chemical reactions begin to play the role of destroying that species.

In particular, the new analysis of CH^+ destruction channel (eq 3) stems from the quantum calculations of the reactive cross section using an accurate RPES that was made available to us from the recent literature[23] and employs a quantum reactive method, the NIP approach used by us before,[35] with a CS treatment of the dynamical coupling during the evolution from reagents to products. A detailed comparison of our new findings with the available experiments and with all recent calculations of the same reaction (see details in section 3 and Figure 2) turns out to indicate that our calculated rates are in very good agreement with experiments and also with the best available quantum calculations for the same destruction reaction over the range of astrophysically relevant temperatures. Furthermore, given the differences shown by all existing calculations (old and new) with the experiments for the low-T data,[15] and to check a possible physical cause of the rate values reduction at the low temperatures (Figure 2), we have also carried out a numerical experiment whereby the barrier in the product region, caused by the avoided crossings at the different orientations of the regents (Figure 1), is artificially modified in height and the ensuing reactive probabilities are analyzed. We thus found that any role of such a barrier in driving the destruction reaction is very relevant in the low-T region, becoming negligible as the temperature is increased. We could therefore suggest from such computations that the low-T behavior of the reaction rates for this system are indeed sensitive to specific details of the diabatization of a multiple-RPES reaction. It will translate, in the experiments, into the possible role of nonadiabatic effects that would be very delicate to measure reliably in that region. Additionally, our detailed modeling of two distinct astrophysical environments, within which reaction 3 is linked to a broader range of chemical processes, has shown that the low-T regimes of the latter reaction play a marginal role for describing its evolution, which is instead dominated by the high-T behavior where our quantum calculations indeed match existing experiments.

The second aspect of the CH^+ chemistry that we have analyzed in some detail and described in the previous section 4 has been the monitoring of its evolution with different visual extinction values (A_v) to model either the high temperature conditions of a PDR environment with intense photon flux (low A_v values) or the low-temperature conditions of a photon-thick environment for a MC. In both cases, at each A_v value the temperature has been kept constant and the additional presence of other radical atoms and ions (together with all their interconnected reactions) has been included in our simulations by accessing the databases UMIST and KIDA. The time evolution has been evaluated by using our own, and now publicly available package KROME.[44] We evolved the kinetic equations for a time of 10^8 years, and the results were collected in Figures 5−7.

From those data we were able to understand that the role of the present destruction reaction is an important one in the PDR conditions whereas, as the temperature and the photon flux decrease, other destruction reactions take over and therefore, to introduce even large changes of the size of the destruction rates for the present reaction, play an overall minor role within those ISM environments.

In conclusion, we should be reminded that our calculated rate coefficients could play a key role at lower temperatures in the H-dominated conditions like those encountered in the cold neutral medium (CNM) regions, where the differences in the CH^+ evolution are expected to be controlled by the destruction reaction studied in this work and over the range of T we are providing.

AUTHOR INFORMATION

Corresponding Author

*F. A. Gianturco. E-mail: Francesco.Gianturco@uibk.ac.at.

Notes

The authors declare no competing financial interest.

ACKNOWLEDGMENTS

We are grateful to Dr. Mario Tacconi for his generous help in the calculations of Figure 3. S.B. is thankful for the funding through the DFG priority programme "The Physics of the Interstellar Medium" (project SCHL 1964/1-1 and BO 4113/1-2). One of us (T.G.) also thanks CINECA consortium of the awarding of financial support while the present research was carried out and the Centre for Star and Planet Formation funded by the Danish National Research Foundation, which partially funded this work. We are very grateful to Robert Warmbier for having provided the PES and shared his results and to Dominik Schleicher for having read this Manuscript and for his useful suggestions on the presentation of our results.

REFERENCES

(1) Douglas, A. E.; Herzberg, G. Note on CH^+ in Interstellar Space and in the Laboratory. *Astrophys. J.* **1941**, *94*, 381.

(2) Crane, P.; Lambert, D. L.; Sheffer, Y. A Very High Resolution Survey of Interstellar CH and CH^+. *Astrophys. J., Suppl. Ser.* **1995**, *99*, 107.

(3) Weselak, T.; Galazutdinov, G. A.; Musaev, F. A.; Kreowski, J. The relation between CH and CN molecules and carriers of 5780 and 5797 diffuse interstellar bands. *Astron. Astrophys.* **2008**, *484*, 381−388.

(4) Kessler, M. F.; Steinz, J. A.; Anderegg, M. E.; Clavel, J.; Drechsel, G.; Estaria, P.; Faelker, J.; Riedinger, J. R.; Robson, A.; Taylor, B. G.;

DOI: 10.1021/acs.jpca.5b02785
J. Phys. Chem. A XXXX, XXX, XXX−XXX

Ximénez de Ferrán, S. The Infrared Space Observatory (ISO) mission. *Adv. Space Res.* **1996**, *315*, L27−L31.
(5) Pilbratt, G. L.; Riedinger, J. R.; Passvogel, T.; Crone, G.; Doyle, D.; Gageur, U.; Heras, A. M.; Jewell, C.; Metcalfe, L.; Ott, S.; Schmidt, M. Herschel Space Observatory. An ESA facility for far-infrared and submillimetre astronomy. *Astron. Astrophys.* **2010**, *518*, L1.
(6) Falgarone, E.; et al. $CH^+(1-0)$ and $^{13}CH^+(1-0)$ absorption lines in the direction of massive star-forming regions. *Astron. Astrophys.* **2010**, *521*, L15.
(7) Godard, B.; Cernicharo, J. A complete model of CH^+ rotational excitation including radiative and chemical pumping processes. *Astron. Astrophys.* **2013**, *550*, A8.
(8) Godard, B.; Falgarone, E.; Des Forêts, G. Pineau Des Forêts,G. Models of turbulent dissipation regions in the diffuse interstellar medium. *Astron. Astrophys.* **2009**, *495*, 847−867.
(9) Wakelam, V.; et al. A KInetic Database for Astrochemistry (KIDA). *Astrophys. J., Suppl. Ser.* **2012**, *199*, 21.
(10) McElroy, D.; Walsh, C.; Markwick, A. J.; Cordiner, M. A.; Smith, K.; Millar, T. J. The UMIST database for astrochemistry 2012. *Astron. Astrophys.* **2013**, *550*, A36.
(11) McEwan, M. J.; Scott, G. B. I.; Adams, N. G.; Babcock, L. M.; Terzieva, R.; Herbst, E. New H and H_2 Reactions with Small Hydrocarbon Ions and Their Roles in Benzene Synthesis in Dense Interstellar Clouds. *Astrophys. J.* **1999**, *513*, 287−293.
(12) Larsson, M.; Orel, A. E. *Dissociative Recombination of Molecular Ions*; Cambridge University Press: Cambridge, U.K., 2008; ISBN 978-0-521-82819-2 (HB).
(13) Mitchell, J. B. A. The dissociative recombination of molecular ions. *Phys. Rep.* **1990**, *186*, 215−248.
(14) Barinovs, Ğ.; van Hemert, M. C. CH^+ Radiative Association. *Astrophys. J.* **2006**, *636*, 923−926.
(15) Plasil, R.; Mehner, T.; Dohnal, P.; Kotrik, T.; Glosik, J.; Gerlich, D. Reactions of Cold Trapped CH^+ Ions with Slow H Atoms. *Astrophys. J.* **2011**, *737*, 60.
(16) Zanchet, A.; Godard, B.; Bulut, N.; Roncero, O.; Halvick, P.; Cernicharo, J. $H_2(v = 0,1) + C^+(^2P) \rightarrow H+CH^+$ State-to-state Rate Constants for Chemical Pumping Models in Astrophysical Media. *Astrophys. J.* **2013**, *766*, 80.
(17) Elitzur, M.; Watson, W. D. Formation of molecular CH^+ in interstellar shocks. *Astrophys. J.* **1978**, *222*, L141−L144.
(18) Draine, B. T.; Katz, N. Magnetohydrodynamic shocks in diffuse clouds. II - Production of CH(+), OH, CH, and other species. *Astrophys. J.* **1986**, *310*, 392−407.
(19) Gredel, R.; van Dishoeck, E. F.; Black, J. H. The abundance of CH(+) in translucent molecular clouds - Further tests of shock models. *Astron. Astrophys.* **1993**, *269*, 477−495.
(20) Crawford, I. A. Ultra-high-resolution observations of the intrinsic line profiles of interstellar CH, CH^+ and CN. *Mon. Not. R. Astron. Soc.* **1995**, *277*, 458−470.
(21) Federman, S. R.; Rawlings, J. M. C.; Taylor, S. D.; Williams, D. A. Synthesis of interstellar CH^+ without OH. *Mon. Not. R. Astron. Soc.* **1996**, *279*, L41−L46.
(22) Stoecklin, T.; Halvick, P. Low temperature quantum rate coefficient of the H + CH^+ reaction. *Phys. Chem. Chem. Phys.* **2005**, *7*, 2446.
(23) Warmbier, R.; Schneider, R. *Phys. Chem. Chem. Phys.* **2011**, *13*, 10285.
(24) Bonfanti, M.; Tantardini, G. F.; Martinazzo, R. *J. Phys. Chem. A* **2014**, *118*, 6595.
(25) Grozdanov, T. P.; McCarroll, R. Influence of the alignment of CH^+ ions in reactive collisions with H atoms at very low temperatures. *Chem. Phys. Lett.* **2013**, *575*, 23−26.
(26) Tacconi, M.; Bovino, S.; Gianturco, F. A. Direct and inverse reactions of LiH^+ with He(1S) from quantum calculations: mechanisms and rates. *Phys. Chem. Chem. Phys.* **2012**, *14*, 637.
(27) Baer, M.; Neuhauser, D.; Oreg, Y. A new accurate (time-independent) method for treating reactive collisions: conversion of a scattering problem into a bound problem. *J. Chem. Soc., Faraday Trans.* **1990**, *86*, 1721−1727.
(28) Bovino, S.; Tacconi, M.; Gianturco, F. A. LiH destruction by protons: a comparison of quantum models for an important astrochemical process. *Phys. Scr.* **2011**, *84*, 028103.
(29) Halvick, P.; Stoecklin, T.; Larrégaray, P.; Bonnet, L. Cross sections and low temperature rate coefficients for the H + CH^+ reaction: a quasiclassical trajectory study. *Phys. Chem. Chem. Phys.* **2007**, *9*, 582.
(30) Jin, Z.; Braams, B. J.; Bowman, J. M. An ab Initio Based Global Potential Energy Surface Describing $CH5^+ \rightarrow CH3^+$+ H2. *J. Phys. Chem. A* **2006**, *110*, 1569−1574.
(31) Wang, Y.; Carter, S. *J. Chem. Phys.* **2008**, *128*, 80.
(32) J, M. *Molecular Potential Energy Functions*; Wiley-Interscience: New York, 1984.
(33) Huarte-Larrañaga, F.; Giménez, X.; Lucas, J. M.; Aguilar, A.; Launay, J.-M. Exact quantum 3D cross sections for the $Ne+H2^+ \rightarrow NeH^+$+H reaction by the hyperspherical method. Comparison with approximate quantum mechanical and classical results. *Phys. Chem. Chem. Phys.* **1999**, *1*, 1125−1132.
(34) Skouteris, D.; Castillo, J. F.; Manolopoulos, D. E. ABC: a quantum reactive scattering program. *Comput. Phys. Commun.* **2000**, *133*, 128−135.
(35) Bovino, S.; Tacconi, M.; Gianturco, F. A.; Galli, D. Ion chemistry in the early universe. Revisiting the role of HeH^+ with new quantum calculations. *Astron. Astrophys.* **2011**, *529*, A140.
(36) Khare, V.; Kouri, D. J.; Baer, M. Infinite order sudden approximation for reactive scattering. I. Basic l-labeled formulation. *J. Chem. Phys.* **1979**, *71*, 1188−1205.
(37) McGuire, P. Validity of the coupled states approximation for molecular collisions. *Chem. Phys.* **1976**, *13*, 81−94.
(38) McGuire, P.; Kouri, D. J. Quantum mechanical close coupling approach to molecular collisions. j_z -conserving coupled states approximation. *J. Chem. Phys.* **1974**, *60*, 2488−2499.
(39) Federer, W.; Villinger, H.; Tosi, P.; Bassi, D.; Ferguson, E.; Lindinger, W. In *Molecular Astrophysics*; Diercksen, G., Huebner, W., Langhoff, P., Eds.; NATO ASI Series; Springer: Netherlands, 1985; Vol. *157*, pp 649−655.
(40) Federer, W.; Villinger, H.; Howorka, F.; Lindinger, W.; Tosis, P.; Bassi, D.; Ferguson, E. Reaction of O^+, CO^+, and CH^+ Ions with Atomic Hydrogen. *Phys. Rev. Lett.* **1984**, *52*, 2084−2086.
(41) Luca, A.; Borodi, G.; Gerlich, D. *Photonic, Electronic and Atomic Collisions: Proceedings of the XXIV International Conference*; World Scientific: Shanghai, 2005.
(42) Röllig, M.; et al. A photon dominated region code comparison study. *Astron. Astrophys.* **2007**, *467*, 187−206.
(43) Tielens, A. G. G. M. *The Physics and Chemistry of the Interstellar Medium*; Cambridge University Press: Cambridge, U.K., 2005; ISBN 0521826349.
(44) Grassi, T.; Bovino, S.; Schleicher, D. R. G.; Prieto, J.; Seifried, D.; Simoncini, E.; Gianturco, F. A. KROME - a package to embed chemistry in astrophysical simulations. *Mon. Not. R. Astron. Soc.* **2014**, *439*, 2386−2419.
(45) Hindmarsh, A. C.; Brown, P. N.; Grant, K. E.; Lee, S. L.; Serban, R.; Shumaker, D. E.; Woodward, C. S. *ACM Trans. Math. Softw.* **2005**, *31*, 363.
(46) Cardelli, J. A.; Mathis, J. S.; Ebbets, D. C.; Savage, B. D. Abundance of interstellar carbon toward Zeta Ophiuchi. *Astrophys. J.* **1993**, *402*, L17−L20.
(47) Meyer, D. M.; Jura, M.; Cardelli, J. A. The Definitive Abundance of Interstellar Oxygen. *Astrophys. J.* **1998**, *493*, 222−229.
(48) Wakelam, V.; Herbst, E. Polycyclic Aromatic Hydrocarbons in Dense Cloud Chemistry. *Astrophys. J.* **2008**, *680*, 371−383.
(49) Draine, B. T. Photoelectric heating of interstellar gas. *Astrophys. J., Suppl. Ser.* **1978**, *36*, 595−619.
(50) Glover, S. C. O.; Jappsen, A.-K. Star Formation at Very Low Metallicity. I. Chemistry and Cooling at Low Densities. *Astrophys. J.* **2007**, *666*, 1−19.
(51) Etxaluze, M.; et al. Herschel spectral mapping of the Helix nebula (NGC 7293). Extended CO photodissociation and OH^+ emission. *Astron. Astrophys.* **2014**, *566*, A78.

DOI: 10.1021/acs.jpca.5b02785
J. Phys. Chem. A XXXX, XXX, XXX−XXX

(52) Mladenović, M.; Roueff, E. Ion−molecule reactions involving HCO^+ and N_2H^+: Isotopologue equilibria from new theoretical calculations and consequences for interstellar isotope fractionation. *Astron. Astrophys.* **2014**, *566*, A144.
(53) Levine R, B. R. *Molecular reaction dynamics and chemical reactivity*; Oxford University Press: Oxford, U.K., 1987.

DOI: 10.1021/acs.jpca.5b02785
J. Phys. Chem. A XXXX, XXX, XXX−XXX